J Mater Sci (2007) 42:7939–7949
DOI 10.1007/s10853-006-1487-4

Synthesis of diamond from a chlorinated organic substance under hydrothermal conditions

Sergiy Korablov · Kazunori Yokosawa · Taku Sasaki · Dmytro Korablov · Akira Kawasaki · Koji Ioku · Emile H. Ishida · Nakamichi Yamasaki

Received: 18 November 2005 / Accepted: 26 December 2006 / Published online: 24 May 2007

Abstract Hydrothermal growth of diamond particles and films was achieved during interaction of a liquid organic precursor ($C_2H_3Cl_3$) and 10 M NaOH in the presence of diamond or cubic BN seeds at the temperature 300 °C and 1 GPa pressure. Synthesized diamond was thoroughly characterized by TG-DTA, SEM, EDX, TEM, Raman spectroscopy and had (220) preferable orientation according to XRD pattern in the case of the film.

Introduction

At present a diamond is effectively produced at high pressures and temperatures (HPHT) from a melt of carbon and catalyst-solvent [1]. In contrast, diamond in the low-pressure region is formed through a vapour phase (CVD). For this process an excited mixture of hydrocarbons and hydrogen is often used [2]. Direct transformation of graphite to diamond under shock wave was also accomplished [3].

However, unique physical and chemical properties of diamond are used only in selected applications due to high costs and limited sizes of both synthetic and natural single crystals. Moreover, the question about natural diamond genesis is still debated, and an accumulation of knowledge in alternative methods of diamond growth continues. Recently, some attempts to overcome the limitations of usual synthesis methods through radically different processes, for example, rapid non-hydrostatic compression of C_{60} at room temperature [4], positionally controlled diamond mechanosynthesis at room temperature by scanning probe microscope [5], extracting silicon from silicon carbide in chlorine-containing gases at ambient pressure [6], and selective leaching of silicon carbide by high-pressure, high-temperature water [7] have been done.

It is very attractive to grow the diamond hydrothermally similar to quartz or emerald [8] and *P–T* conditions of such a process could be between HPHT and CVD processes.

At present, extensive research on diamond synthesis by CVD has been accomplished and considerable technical progress was achieved. A possibility of diamond crystal growth during CVD process under oxygen-containing environment [9, 10] is also important for the hydrothermal method. Exposure to hostile atmosphere and preferential etching of different facets are proposed to be the main causes for the formation of diamond films at these conditions. Moreover, an addition of 1.3 vol.% of water to methane–hydrogen gas leads to rapid growth of diamond particles. The effect of water is considered as a promotion of the methane decomposition and graphite removal reactions [11].

Microdiamonds (size range 0.07–0.2 mm) from garnet clinopyroxenites of the Kokchetav massif (northern Kazakhstan) were first discovered in 1967 [12]. Further inquiry of microdiamonds from Kazakhstan, China, Norway and Germany in the last decade [13–17] revealed that they contain abundant Ib centers [13, 17], have high

S. Korablov (✉) · K. Yokosawa · T. Sasaki · D. Korablov · K. Ioku · E. H. Ishida · N. Yamasaki
Department of Environmental Studies, Graduate School of Environmental Studies, Tohoku University, Aramaki, Aoba ku, Sendai 980-8579, Japan
e-mail: sergiy2@yahoo.com

A. Kawasaki
Department of Materials Processing, Graduate School of Engineering, Tohoku University, Aramaki, Aoba ku, Sendai 980-8579, Japan

nitrogen content and led to unexceptional assertion that these diamonds are derived from another host rock than a kimberlite. Characterization of the polyphase inclusions in these microdiamonds revealed that these aggregates represent the original inclusions of a supercritical dense C–O–H fluid rich in alkali and silica [14] or carbonate–water–nitrogen mixture [17]. From these fluids the diamond was precipitated as a daughter crystal due to cooling at the ultrahigh pressure metamorphic conditions ($P > 4.5$ GPa, at 1,000 °C) [16]. Conditions for crystallization of microdiamond were proposed by other authors [17] as follows: pressure 2.7–3.5 GPa and temperature 500–700 °C.

In spite of the fact that microdiamond has been known for a long time and DeVries et al. [18] conducted a comprehensive review of various carbon–liquid systems closely related to the synthesis of diamond, there are only a few attempts of practical hydrothermal growth of diamond [19–23]. Chemical composition of reactant solutions [22, 23] coincides with the growing environment for microdiamonds in nature [14, 16] and in laboratory conditions [7]. However, the composition of aqueous solution was not reported [20, 21]. Moreover, results of selective leaching of silicon carbide by HPHT water [7] as well as hydrothermal growth of diamond in metal–C–H_2O systems [19] represent the growth in supercritical solutions, because in both methods the temperature was 800 °C at pressures 100 and 140 MPa, respectively.

The chemical mechanisms controlling the growth, nucleation and epitaxy of diamond in thermodynamically metastable environments are not completely understood yet, however, some observations indicate that intermediate diamond-forming species are a common decomposition product of the original source phase [2]. Perhaps, processes of gas phase and liquid phase epitaxy could be very similar to each other [21]. The surface reactions and steady-state surface structure of the substrate are important in both cases.

Diamond appears in the sequence of thermal decomposition of organic compounds (polycyclic aromatic hydrocarbons [24]) through carbonization and pressure-induced polymerization at temperatures above 1,280 °C and pressures of at least 8 GPa. On the other hand the chlorinated organic compounds (COC) are easily decomposed under moderate alkaline hydrothermal conditions [25] that allow a COC–NaOH–seed system as a possible model for study of diamond formation in high-pressure hydrothermal conditions.

In this paper, the synthesis of diamond structured carbon by high-pressure low-temperature (HPLT) epitaxy of seeds through the hydrothermal reaction of liquid reagents according to P–T conditions [26] was produced and discussed on the base of characters of CVD growth.

Experimental details

Materials

As noted in Ref. [8], it is difficult to prove the new growth of diamond in the presence of diamond seeds [19, 21]. Therefore, our approach was to conduct a hydrothermal reaction at the artificially created surface. Therefore, several pellets containing 2 g/cm^3 of 1 μm average size (5,000 mesh) or 4 g/cm^3 of 45 μm average size (325 mesh) natural diamond seeds (both Osaka Diamond Industrial Co., Ltd) have been prepared by mixing with Cu powder (Wako Pure Chemical Industries, Ltd.) and pressing in a steel mold with a 150 MPa load. In this case the new growth can easily occur only on the surface of pellets and perhaps continue as a film. Prior to the growth experiments, diamond seeds were hydrogenated according to Ref. [27].

However, a probability still remains that the initial diamond seeds will be absorbed by the growing layer and will make an impact on the results of study. Therefore, the process was also realized with a substrate another than diamond. In this case the 45 μm (325 mesh) cubic BN (Sumitomo Electric Industries Ltd.) pre-treated in H_2 plasma was used as seeds.

Hydrothermal reaction has been fulfilled in a piston-cylinder device [28]. Two types of copper container 0.6 and 7.0 ml volume (Fig. 1) were used in our experiments.

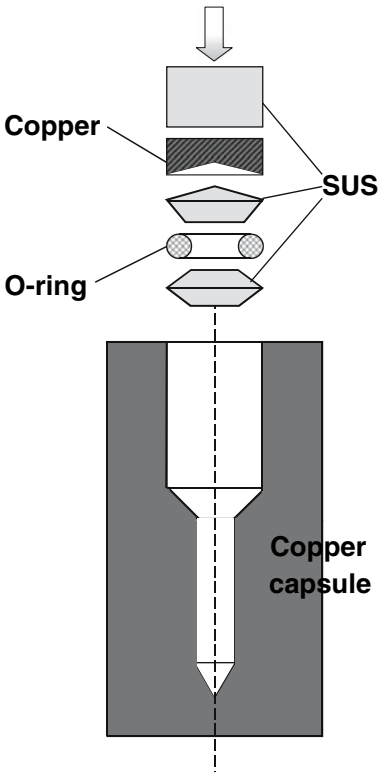

Fig. 1 Scheme of packing of capsule

Hydrogenated diamond powder and/or Cu-containing seeds were placed on the bottom of the copper container with the following liquids reagents: a carbon precursor and 10 M NaOH (Wako Pure Chemical Industries, Ltd.) in proportion 1:(0.3–3). The chlorinated organic compounds (COC): a 1,1,1-Trichloroethane ($C_2H_3Cl_3$), hexachlorocyclohexane ($C_6H_6Cl_6$) or dichloromethane (CH_2Cl_2) (all Wako Pure Chemical Industries, Ltd.) were used as the carbon source. Starting COC compounds have the same number of hydrogen and chlorine atoms in each molecule allowing removal of both as HCl and producing pure carbon as the result of the decomposition reaction.

The sealed copper container was loaded at the pressure range 0.7–2.5 GPa in the piston-cylinder type high-pressure vessel and then slowly heated in the temperature interval 100–300 °C with a differing heating rate (0.1–1.2°/min). The typical experiment was conducted at the following conditions: pressure 1 GPa, temperature 300 °C and exposure 72 h. After 1–3 days exposure the reaction products were divided into gas, liquid and solid portions. The latter was ultrasonically cleaned in distilled water and acetone, and then two steps of acid treatment were applied. Ballast products NaCl, $CuCl_2 \cdot Cu(OH)_2$, and NaCuO were eliminated after treatment in Aqua regia during 24 h at room temperature.

Hydrothermal conditions are far from equilibrium for diamond growth, therefore some non-diamond carbon naturally appears. For effective removal of amorphous carbon we used two approaches. One was boiling in a mixture of sulfuric acid and $K_2Cr_2O_7$ for 2–4 h. Another was an elimination of surface non-diamond carbon by oxidation in air.

Characterization

The resistance of different forms of hydrothermal carbon to air oxidation was determined by a Rigaku Thermoplus TG-8120 on the basis of differential thermal analysis (DTA) coupled with thermo-gravimetry measurement (TG).

The surface of the hydrothermal reaction products and their chemical composition were inspected by a scanning electron microscope (SEM) Hitachi S-4700T equipped with an energy dispersive X-ray spectrometer (EDX).

In the case of micro X-ray diffraction (μ-XRD) analysis a monochromatic CuK_α radiation was used with a 30 μm collimator (JEOL JDX-3530) or a 100 μm collimator (M21X MAC Science Co., Ltd).

Selected reaction products were examined by a JEM 200CX transmission electron microscope (TEM) operating at 200 kV.

The Raman analyses were conducted using a Caiser Optical Systems Hololab 5000 spectrometer at an argon laser wavelength of 532.07 nm.

Reaction products dissolved in water were analyzed by a Hiranuma TOC-2000 Total Organic Carbon analyzer and those dissolved in acetone (*n*-hexane) were subjected to gas chromatography using a Hewlett Packard 5890-GC system with a 5989B mass spectrometric detector (GC-MC).

Residual gases were tested using a Hitachi G-3900 Gas Chromatograph with split injection.

Results and discussion

Experiments without seeds

Several kinds of hydrothermal carbon products were collected in these experiments. For example, black shiny pieces, black powder, and brown low-density carbon floating on the water surface were produced in large quantities after 24 h of exposure at 1 GPa and 300 °C. These samples are characterized by a series of strong and/or overlapping exothermic effects in the temperature range 320–570 °C and completely burned out at 600 °C during high temperature oxidation in air. Regardless of different organic precursors, all of them were amorphous according to XRD data and contained a lot of magnetite (Fe_3O_4) before Aqua regia treatment at 100 °C for 2 h. It is important that transparent oxide crystals with different morphology were also elicited from the inside of the carbon species after burning of the latter in air or dissolution in a mixture of sulfuric acid and $K_2Cr_2O_7$. This means that magnetite crystals were formed as a result of electrochemical corrosion between SUS (stainless steel) plug and copper container (Fig. 1), and then a catalytic decomposition of organic precursor occurred on their surface.

In fact the formation of amorphous carbon means that the diamond growth is restricted because at the studied conditions there are no real driving forces to change the stable amorphous phase to diamond. Consequently, for diamond growth it is necessary to delay the formation of amorphous carbon and to provide a liquid-state precursor for a long time. For example, at the same experiment conditions the elimination of the electrochemical corrosion process in the case of the copper packing container instead of stainless steel packing (Fig. 1) leads to a 3-fold decrease of amorphous carbon yield. Therefore, the steel stopper was isolated from the reaction volume by the copper foil in future experiments.

Experiments with uncombined seeds

Free sintering of small diamond particles

Similar to CVD growth, the hydrothermal conditions are far from equilibrium for diamond growth and, therefore, a

certain activation of the process is required. For example, availability of diamond seeds can reduce an energy barrier for direct deposition of diamond from the liquid organic precursor.

Experiments were performed in pure copper surroundings with 1,1,1-Trichloroethane, NaOH and 1 μm hydrogenated diamond seeds as reagents using the following conditions: 1 GPa, 300 °C, and 72 h. It was found that after the experiment an excess of pressure inside of the capsule is mostly a result of gaseous products. Residual amounts of liquid were very small; therefore, the main hydrothermal process was already stopped. After two steps of acid treatment the solid reaction product had a white color and averaged only about 11% of by-product. Thus, a low ratio of active component to ballast makes this process similar to CVD growth.

Unfortunately, we could not confirm the new diamond formation by weight measurement due to a loss of some amount of reaction products during the treatment process. Moreover, the refined reaction product did not reveal any differences in X-ray diffraction and Raman shift data in comparison with the initial diamond seeds. However, air oxidation resulted in some features become discernible. The results of DTA are shown in Fig. 2. The hydrogenation of the initial diamond causes a shift of the oxidation reaction rate maximum (708 °C DTA effect) to a higher temperature region in comparison with the initial seeds. The increase of oxidation resistance occurs due to removal of the surface defects during hydrogenation at high temperatures. The hydrothermal synthesis products are characterized by small amounts of amorphous carbon, which completely burned at 600 °C. A peak at 727 °C corresponds to 1 μm hydrogenated diamond seeds. However, the peak at 858 °C is important because it means that some coarse diamond grains appeared. Thus, DTA data are very effective for separation of different carbon materials.

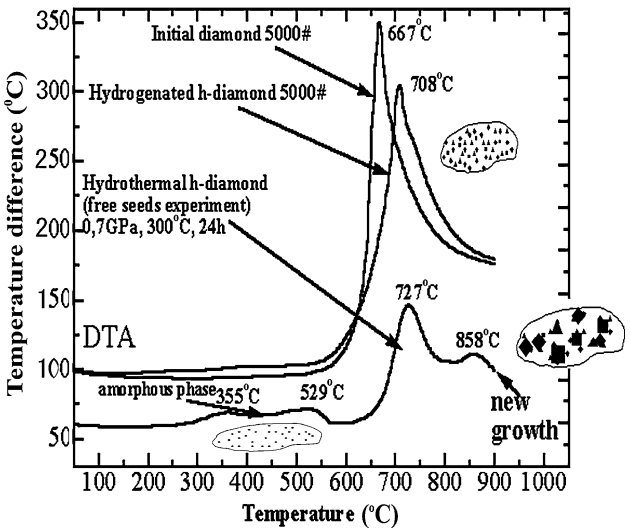

Fig. 2 DTA curves of non-isothermal oxidation in air with a heating rate of 10°/min. Hydrothermal h-diamond was subjected to a two-step acid treatment

Moreover, during modeling tests we have found that DTA is sufficiently sensitive to grain size of diamond subjected to air oxidation and we have been able to separate thermal effect from the coarse diamond grains mixed with fine grains.

The assumption about coarsening of initial seeds through hydrothermal reaction was confirmed after careful optical and electron microscopy studies of the samples treated with two steps of acid processing. Figure 3 demonstrates the scanning electron microscopy images of transparent and strong diamond polycrystals shaped as globules, and initial seeds at approximately the same magnification. It is obvious that globules were produced through free sintering of initial 1 μm seeds (Fig. 4a), and according to EDX they have no impurities besides carbon and oxygen similar to initial h-diamond seeds (Fig. 4b and c).

It should be noted that if the ratio of NaOH:TCE exceeded 3, we did not observe any changes of the seeds.

Experiments with 45 μm diamond seeds

In the case of 45 μm hydrogenated diamond seeds we did not reach the sintering of these coarse grains. However, less than 1 μm small particles were produced from the hydrothermal reaction product after a two-step acid treatment. Morphology of these particles (Fig. 5a) differs from the typical faceted shape of HPHT or natural diamond, but is often observed in CVD films [29, 30]. Moreover, spherical nanodiamonds are energetically favored at the nanoscale size [31]. Transmission electron microscopy studies show that these particles consist of diamond (Fig. 5b–d) cubic Fd3m with reflection at 0.206 nm or 2H hexagonal (lonsdaleite) (Fig. 5c) with 0.193 nm lattice spacing. According to Ref. [32], studied particles are not a result of destruction of initial seeds because the diamond is undoubtedly in the stable phase at the moderate *P–T* conditions used in the experiment. Further, selected initial seeds did not contain any small grains and had a low level of surface defects due to hydrogen pre-treatment at 850 °C.

Liquid phase homoepitaxy of large crystals

If we replaced the fine diamond seeds by 3–5 large (500–800 μm size) diamond crystals then small areas as decoration of diamond epitaxial growth were observed on the seeds surface at high magnification (Fig. 6) after hydrothermal treatment and did not appear before. The new diamond growth has been detected as specific layer plus island growth structure (Fig. 6b and c).

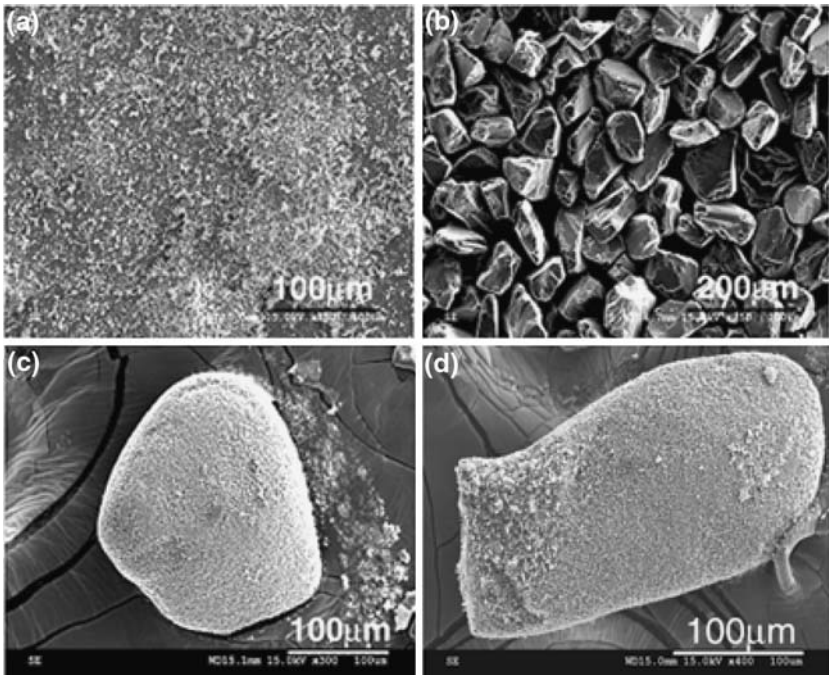

Fig. 3 SEM images of hydrothermal synthesis products after two steps acid treatment (**c**, **d**) and initial seeds: 1 μm (**a**) and 45 μm (**b**)

In general, an octahedron is the most common [33] and equilibrium growth form for diamond [34], however, most natural diamond have morphologies that are intermediate between octahedral {111}, dodecahedral {110}, and more rarely cubes {100} or twins [35]. Tetrahedral diamonds are exceedingly rare and such crystals show apparent tetrahedral symmetry [36]. HPHT diamond grown from various metal solvents or carbonates displays {111} and {100} persistent faces whereas {110} and {113} faces are transient [37, 38]. Different morphologies of CVD diamonds are observed depending upon deposition conditions. Equilibrium growth results in {111} faces as a growing surface. As deposition conditions vary from equilibrium {100} cube faces appear [34], but generally morphology is more complex [39, 40]. New growth in Fig. 6c demonstrates a flat and smooth deposited diamond layer similar to CVD homoepitaxial growth [41]. However, it is very difficult to clearly estimate the morphology of the island growth structure due to small size and great number of hillocks, but obviously these are step layered octahedral crystals. The growth of the diamond phase as a layer and non-diamond inclusions only as islands during deposition of C_2 molecules onto the diamond (110) surface was discussed in Ref. [42].

Diamond platelets

After experiments with fixed seeds, small transparent platelets, which were brittle like ceramics and considerably differed in size, shape and surface morphology from the seeds used, were found. They were elicited from the acid treated reaction products (Fig. 7a–d). These carbon based 200–500 μm size platelets (average size of used seeds was 1 or 45 μm) are certainly new growth, characterized by increased oxygen concentration (Fig. 7e–g) in comparison with seeds and sintered globules (Fig. 4b and c). Furthermore, these platelets have exhibited stability in air oxidation conditions at temperatures up to 1,000 °C with a heating rate 10°/min similar to coarse 45 μm diamond seeds. Figure 7c and d, f and g show the surface structure of two large hydrothermal carbon platelets after air oxidation with corresponding EDX spectra. One reveals the homogeneous structure, but another has large zones of low-density carbon (Fig. 7d and g), which has been selectively removed during the reaction with oxygen at high temperature. The high temperature oxidation provides the formation of a typical skeletal structure, which is most likely for microdiamonds separated from garnets [15]. Moreover, similar to natural microdiamonds, the skeletal plate has discernible amount of silica (Fig. 7g), obviously due to contamination of the liquid reagents.

Sufficiently large size permitted the X-Ray analysis for each carbon platelet. According to μ-XRD data (Fig. 8) these platelets contained amorphous or, perhaps, nanocrystalline diamond phase, because the diamond growth outside the region of their thermodynamic stability is preferably continued as nanocrystalline diamond-structured carbon with nanocrystals average size of 5–10 nm [6]. However, some platelets displayed (111) and (220) diamond peaks (Fig. 8b and c) or (220) reflex even after heating up to 1,000 °C in air (Fig. 8b). There is evidence that the CVD growth mainly proceeds on the (110) face

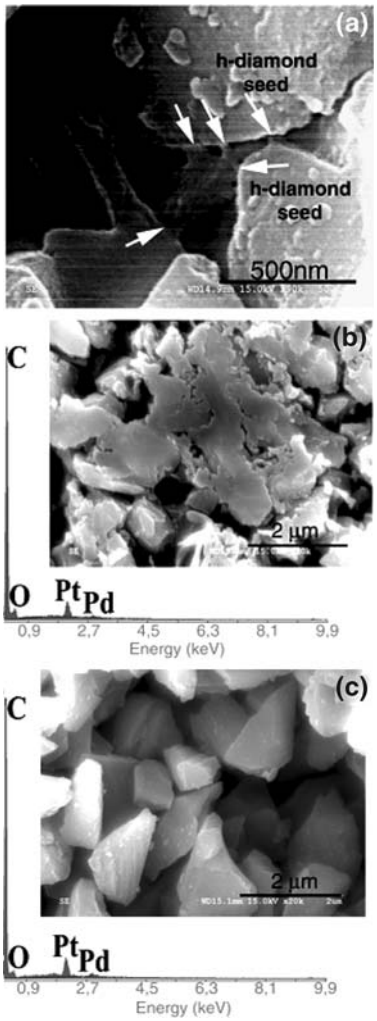

Fig. 4 SEM images of globule shaped diamond polycrystals (**a**, **b**) and 1 μm seeds (**c**) with appropriate EDX data. The new diamond growth between h-diamond seeds is shown in (**a**) by arrows

[43, 44], and, obviously, this is a reason why hydrothermal products mostly revealed (220) reflection in μ-XRD patterns while starting seeds demonstrate a maximum intensity for (111) line (Fig. 8a). Of course, during growth the new phase can involve some amount of seeds from the surface of the copper templates. However, we did not find any presence of the initial seeds on the surface of the large platelets, which were analyzed by μ-XRD. Moreover, the number of diamond grains in the surface layer of Cu-pellets was limited and could not be estimated by XRD. In addition, the 1 μm starting diamond powder completely disappeared after heating up to 1,000 °C in air, while hydrothermally produced diamond platelets remained unburned (Figs. 7c–g and 8b). Because the oxidation of any pure carbon, including diamond, is accompanied by a decrease in weight and grain size (reaction products are gases and no solid products are formed [45]), small grains burn out, and large grains, which decrease in size, can be revealed at higher temperatures during programmed heating in air. Newly produced diamond is oxidized in the same manner with initial seeds, however, due to a larger size (200–500 μm) the platelets were found in the unburned residue. These platelets were free of inclusions (metal or other, according to EDX) and therefore have no coating on their surface (after two steps of pre-cleaning).

Experiments with cubic BN seeds

For unambiguous confirmation of diamond growth in our process, we have conducted the Raman analysis (at 532.07 nm laser wavelength) of the reaction products grown on a substrate other than diamond [46]. In this case the 45 μm cubic BN was used as seeds. Raman spectra are shown in Fig. 9. Raman spectrum of c-BN (Fig. 9b) revealed the 1,055 cm^{-1} transverse optical (TO) and 1,305 cm^{-1} longitudinal optical (LO) peaks [47]. Spectrum of the hydrothermal product after the first step of clearance is similar to seedless experiments. The Raman spectrum (Fig. 9c) shows a prominent peak at 1,581 cm^{-1} related to sp^2 bonded carbon vibrations (G band) and a broad peak at 1,348 cm^{-1} that is a disorder-induced D band of graphitic carbon [48]. Completely purified hydrothermal product (Fig. 9d) demonstrates a weak TO peak of the c-BN substrate and a single narrow diamond peak at 1,332 cm^{-1} with the full width at the half maximum (FWHM) value of 5.3 cm^{-1} that gives obvious evidence of the formation of cubic diamond under hydrothermal conditions because the single crystalline diamond grains show only this peak in Fig. 9a with FWHM value of ~6 cm^{-1}.

Analysis of residual gases

Earlier [49], we proposed that the following reaction leads to formation of diamond-bearing species:

$$C_2H_3Cl_3 + 3NaOH = 2C + 3NaCl + 3H_2O \quad (1)$$

However, the reaction (1) is a scale-downed version of hydrothermal process, which occurs at temperatures below 100 °C, because already at 100 °C the gas phase was found in the reaction products. This amount was not enough for classification by gas chromatography, but analysis of data in Fig. 10a permits us to suppose that this is pure hydrogen. At higher temperatures the gas phase reaction products consist of H_2, CH_4, CO and CO_2. The latter was found only after 250 °C but at very low level. Thus, there is a reducing environment for the whole experimental temperature range. Moreover, methane was not observed at temperatures up to 150 °C, and the H_2/CH_4 ratio typical for CVD growth was maintained up to 200 °C.

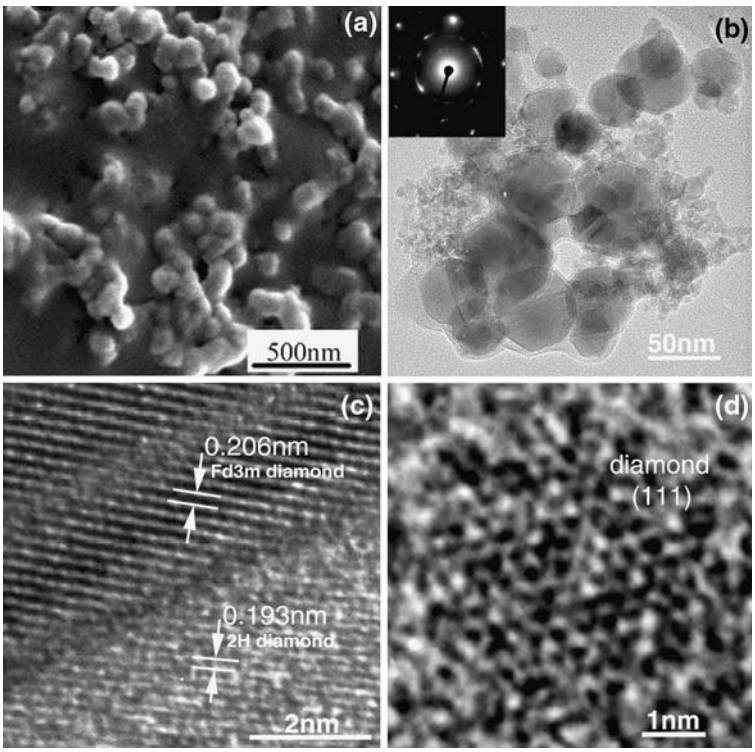

Fig. 5 SEM image (**a**), TEM image with corresponding SAD pattern (**b**) and high-resolution TEM images (**c**, **d**) of hydrothermal diamond produced in experiments with 45 μm h-diamond seeds

According to above-mentioned, it is possible to suppose that following reactions occur

$$\text{below } 150\ ^\circ\text{C}: \quad C_2H_3Cl_3 + 3NaOH = C + H_2 + CO + 2H_2O + 3NaCl \tag{2}$$

$$\text{above } 250\ ^\circ\text{C}: \quad 2C_2H_3Cl_3 + 6NaOH = C + CH_4 + 2CO + 4H_2O + 6NaCl \tag{3}$$

and taking into account all detected phases at 300 °C:

$$2C_2H_3Cl_3 + 6NaOH = C + H_2 + CH_4 + CO + CO_2 + 3H_2O + 6NaCl \tag{4}$$

Analysis of residual liquids

Analysis of the residual liquids on total organic (TOC) or inorganic (TIC) carbon are shown in Fig. 10b. After exposure for 72 h at room temperature, the initial mixture demonstrates mostly inorganic carbon, the concentration of which sharply decreases at 100 °C, and then more gradually decreases up to 350 °C. The total amount of organic carbon is increases dramatically at 100 °C and then decreases at 300 °C with a slower decrease to 350 °C, but remained two times greater than the value of inorganic carbon at 300 and 350 °C for 48 h.

According to the gas chromatography results, the residual organic liquids consist of a mixture of a benzeacetic, propanoic, benzoic and benzeneacetic acid in decreasing order of content and tetradecane. The same liquid organic products as well as residual gases were detected for all COC–NaOH systems.

Hydrothermal conditions pertinent to diamond growth

Analysis of main chemical components

In comparison to reported hydrothermal conditions [7], we have observed the hydrothermal growth of diamond at another part of Bachmann–Rumble diagram, which summarizes the C–H–O range for CVD diamond formation. Our starting reaction medium was enriched by oxygen (Fig. 11) in comparison with a H_2O/SiC interaction [7], and we also found the diamond formation (particles or films) outside of proposed diamond growth region in the Bachmann diagram [18]. After the test at 300 °C, 1 GPa, for 72 h the residual gas mixture revealed more reducing properties, mostly, due to oxygen consumption during the interaction of liquid reagents with the copper container.

It can be supposed that intermediate diamond forming species are common decomposition products of the original source liquids. For example, in Ref. [50] the authors studied the polyethylene (PE) decomposition in supercritical water with a diamond anvil cell (DAC) technique.

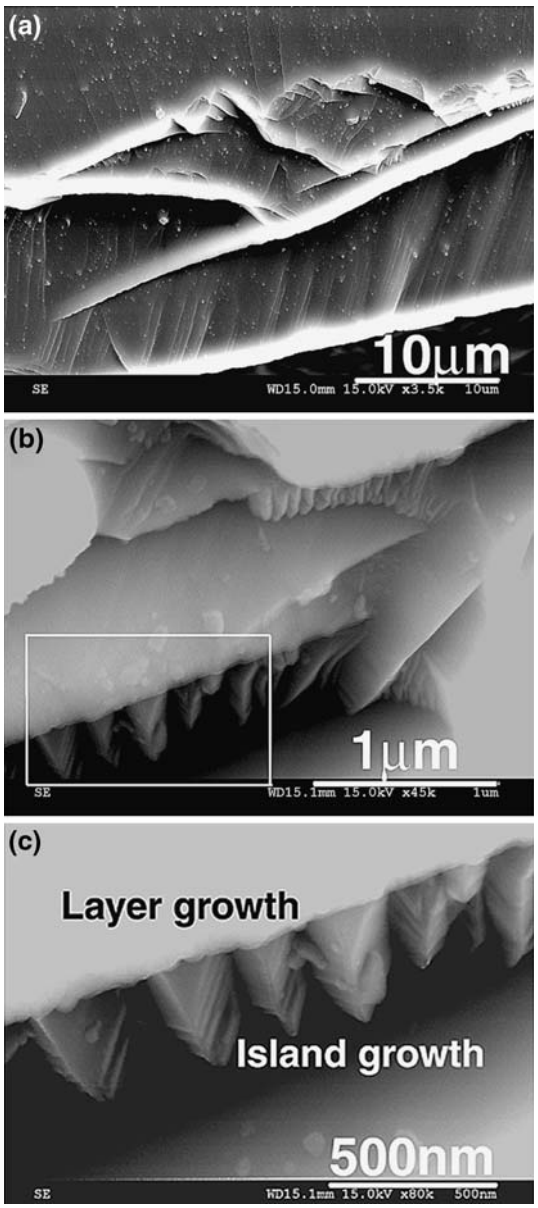

Fig. 6 SEM image demonstrates the surface of a large 500 μm diamond seed after a two-step acid treatment, (**c**) shows the magnified region of the area framed in (**b**) and specific characteristics of the diamond layer produced through liquid phase homo-epitaxy

Raman analysis was attempted but could not be performed due to very high fluorescence of the products. After the sample was cooled down from 560 °C, and the pressure was decreased from 1.75 GPa a film was found on each of the diamond anvils. The films were observed at a temperature interval of 560–670 °C and pressure range from 1.75 to 2.66 GPa and had a very broad and strong C=C (1,607 cm^{-1}) and sharp C–C (1,333 cm^{-1}) Raman bands. Of course, C–C bond vibration occurred at the same position as the diamond anvils, and diamond formation has not been discussed for this process yet. However, the 1,333 cm^{-1} peak was strongly suppressed after the experiment at 423 °C and a pressure of 0.986 GPa. Therefore, products of partial decomposition of polyethylene cover the diamond anvil, and the incident laser beam cannot penetrate beyond this layer due to strong adsorption. This means that the detected 1,333 cm^{-1} Raman peak characterizes the reaction product (not DAC), and the decomposition of polyethylene in supercritical water (in general C–H–O liquid) at the *P–T* parameters near to crystallization of natural microdiamond [16, 17] leads to the formation of sp^3-bonded carbon. Moreover, the authors have used ^{13}C diamond as an indicator of pressure and observed that it curiously jumped across the cell and joined with the PE droplet. Obviously, during decomposition of PE, the intermediate products responsible for diamond growth were formed in large quantity. As a result, the sensor became attached to the molten PE phase.

The role of chlorine and sodium

The role of chlorine is clearly understandable during the formation of diamond structured carbon through extraction of silicon from silicon carbide in chlorine containing gases at ambient pressure [6] or during growth of nanocrystalline diamond films in the CCl_4/H_2 environment in a hot-filament CVD reactor [29, 51], but for hydrothermal growth from COC it is currently unknown. For example, the chemical analysis of pure hydrothermal products (Figs. 4b and 7e–g) did not reveal presence of chlorine or sodium. It was suggested that chlorine of TCE reacts with the hydrogenated diamond surface, and then HCl is removed through a reaction with NaOH [52]. As a result, the single C–C bond should be formed. However, it is clear that TCE decomposed already at 100 °C in alkaline hydrothermal conditions. Obviously, the role of alkali is to produce and stabilize the intermediate diamond forming species.

The role of P–T conditions

Our *P–T* parameters differ from natural microdiamond crystallization conditions. However, the diamond–graphite equilibrium line [16, 17] suggests that pressure near 2 GPa corresponds to the temperature 200–300 °C. If we take into account that the pressure claimed in these experiments (1 GPa) corresponds to 0.7–0.9 units of real pressure applied to the copper capsule, and an enhancement of pressure in the system of about 30% for first 24 h was observed, then our results do not contradict an approximation from Refs. [16, 17].

Moreover, it was found [13, 15] that microdiamond-bearing fluids were highly enriched with oxygen to produce oxidized species, but it was not enough to oxidize the diamond [15]. In general the temperature of 500–700 °C is

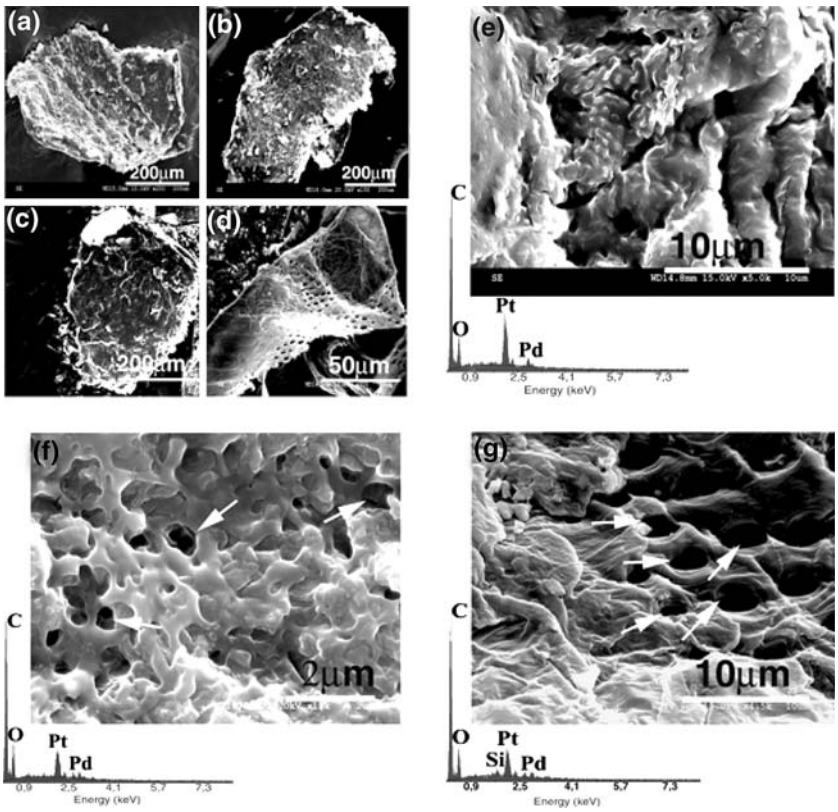

Fig. 7 Low (**a**–**d**) and high-resolution (**e**–**g**) SEM images (with corresponding EDX data) show size, shape, structure and composition of the hydrothermal synthesis products after the two-step acid treatment (**a**, **b**, **e**), and after cleaning in Aqua regia and air oxidation to 1,000 °C (**c**, **d**, **f**, **g**). Arrows indicate holes produced through elimination of low-density non-diamond carbon

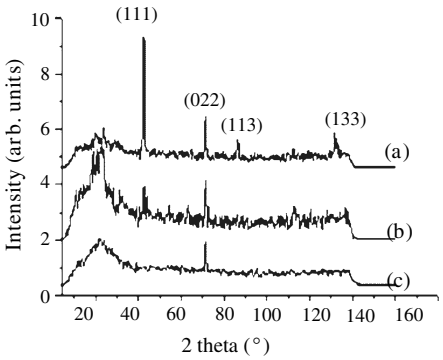

Fig. 8 Micro XRD patterns of hydrothermal carbon platelets (**b**, **c**) and initial 1 μm seeds (**a**); (**b**) after exposure in Aqua regia for 24 h and air oxidation to 1,000 °C; (**c**) after a two-step acid treatment

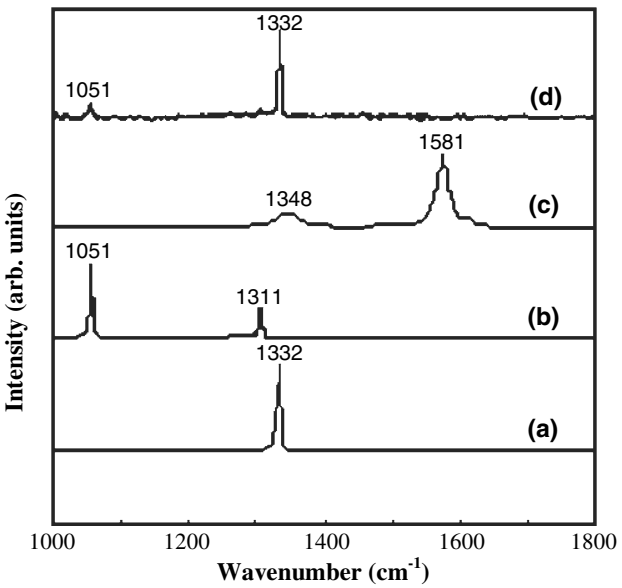

Fig. 9 Raman spectra of the initial diamond seeds (**a**), cubic BN 45 μm seeds (**b**), and hydrothermal products after cleaning in Aqua regia for 24 h (**c**) and after a two-step acid treatment (**d**)

enough for the oxidation of diamond, but by lowering the temperature, for example to 300 °C as in our case, we moved to the range of diamond stability.

Mechanism of hydrothermal growth

The mechanism of hydrothermal growth is not properly understood at this stage. Before we proposed that this mechanism is condensation–polymerization [49]. COC easily decomposes under alkaline hydrothermal conditions [25], as a result the colloidal solution containing unstable and very active carbon could be produced. Diamond growth may then occur by insertion of active C species (reactions 1–4) into C–H bonds of the hydrogen terminated diamond surfaces. For example, the energy barriers for

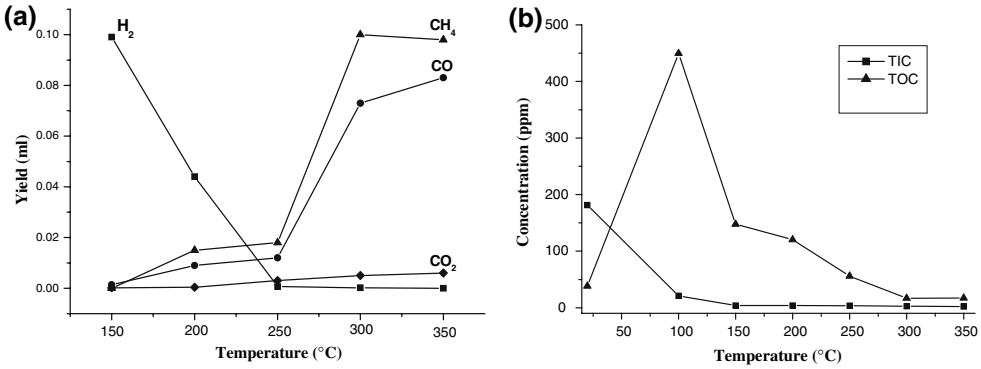

Fig. 10 Composition of residual gases as a function of temperature for the hydrothermal reaction at 1 GPa for 48 h (**a**) and temperature dependencies of the amounts of organic and inorganic carbon in residual liquids after experiments at 1 GPa for 48 h (**b**)

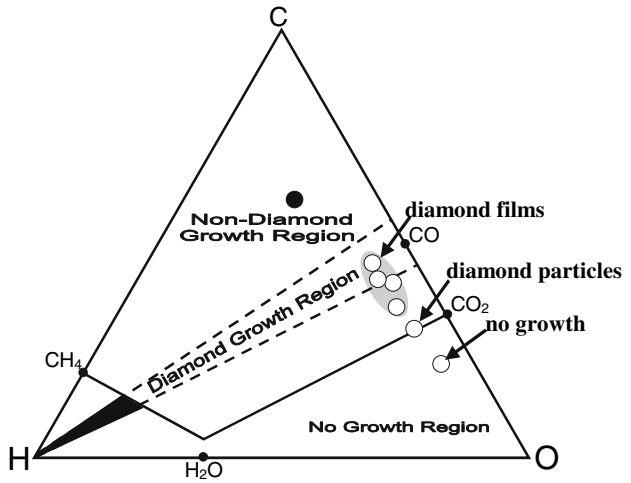

Fig. 11 Bachmann–Rumble diagram with the black triangle corresponding to the hydrothermal conditions for diamond growth [7]. Circles show the regions studied in this work. The black circle corresponds to the C–H–O range for non-diamond films growth

addition of C_2 to diamond surface are small during diamond thin film growth from fullerene precursors, and (110) hydrogen terminated diamond surface [53] or even the bare substrate [42, 53] are energetically very favorable for growth. This is in good agreement with XRD data for hydrothermal diamond (Fig. 8). Moreover, a completion of new diamond layer may proceed via formation of single bonds between ethylene like adsorbate and radical structure [53, 54].

Conclusions

Hydrothermal synthesis of diamond from liquid organic precursor was achieved at moderate *P–T* conditions. Refined reaction products were comprehensively characterized in order to confirm diamond formation.

It should be noted that we did not use any catalyst metals (usual Ni–Fe–Mn or Co). Pure copper is not a catalyst for diamond synthesis [55], and produced diamond is free of metallic elements (according to EDX data) similar to natural diamond [8].

The obtained results coincide with parameters predicted for natural microdiamond formation. Despite the fact that at this stage the intermediate diamond bearing species for hydrothermal growth are still unknown, some data indicate that it should be similar for hydrothermal C–H–O systems in a similar manner with CVD growth.

As diamond structured carbon has been synthesized through high-pressure low-temperature liquid phase epitaxy of seeds, the growth of diamond in nature can continue as cubic diamond formed in kimberlitic magma at the depth 100–250 km moves to near surface layers 1–10 km deep.

Acknowledgements We thank M.R. Davidson (CASE Western Reserve University) for help for preparation of this paper and Prof. Yury Gogotsi (Drexel University) for helpful discussion and editing the manuscript. S. Korablov was supported by a JSPS Research Fellowship.

References

1. Bundy FP, Hall HT, Strong HM, Wentorf RH (1955) Nature 176:51
2. Angus JC, Hayman CC (1988) Science 241:913
3. Burkhard G, Dan K, Tanabe Y, Sawaoka AB, Yamada K (1994) Jpn J Appl Phys 33:L876
4. Regueiro MN, Monceau P, Hadeau J-L (1992) Nature 355:237
5. Merkle RC, Freitas RA (2003) J Nanosci Nanotechnol 3:1
6. Gogotsi YG, Welz S, Ersoy DA, McNallan MJ (2001) Nature 441:283
7. Gogotsi YG, Kofstad P, Yoshimura M, Nickel KG (1996) Diamond Relat Mater 5:151
8. DeVries RC (1997) Nature 385:485
9. Ravi KV (1995) Diamond Relat Mater 4(4):243
10. Kim J-S, Kappelli MA (1995) Surf Coat Tech 76–77:791
11. Saito Y, Sato K, Tanaka H, Fujta K, Matuda S (1988) J Mater Sci 23:842. DOI: 10.1007/BF01153976
12. Dobrzhinetskaya LF, Braun TV, Sheshikel GG, Podkuiko YA (1994) Tectonophysics 233:293
13. DeCorte K, Cartigny P, Shatsky VS, Sobolev NV, Javoy M (1998) Geochim Cosmochim Acta 62(23/24):3765

14. Dobrzhinetskaya LF, Green HW, Wescheer M, Darus M, Wang Y-C, Massone H-J, Stöckhert B (2003) Earth Planet Sci Lett 210:399
15. Dobrzhinetskaya LF, Green HW, Mitchell TE, Diskerson RM (2001) Geology 29(3):263
16. Stöckhert B, Dnyster J, Trepmann C, Massone H-J (2001) Geology 29(5):391
17. Cartigny P, DeCorte K, Shatsky VS, Ader M, DePaepe P, Sobolev NV, Javoy M (2001) Chem Geol 176:265
18. DeVries RC, Roy R, Somiya S, Yamada S (1994) Trans Mat Res Soc Jpn 19B(6):641
19. Zhao X-Z, Roy R, Cherian KA, Badzian A (1997) Nature 385:513
20. Szymanski A, Abgarowicz E, Bacon A, Niedbalska A, Salacinski R, Sentek J (1995) Diamond Relat Mater 4:234
21. Szymanski A (1996) J Chem Vap Depos 4:278
22. Korablov S, Yokozawa K, Tohji K, Yamasaki N (2004) Trans Mat Res Soc Jpn 29(5):2371
23. Yamasaki N, Korablov S, Yokosawa K (2002) In: Proceedings of the 5th international conference on the solvo-thermal reactions, East Brunswisk, NJ, 22–26 July 2002, p 371
24. Davydov VA, Rakhmanina AV, Agafonov V, Narynbetov B, Boudou J-P, Szwarc H (2004) Carbon 42:261
25. Yamasaki N, Yasui T, Matsuoka M (1980) Environ Sci Technol 14:550
26. Sato H, Uematsu K, Watanabe K, Saul A, Wagner W (1988) J Phys Chem Ref Dat 17:1439
27. Tsubota T, Hirabayashi O, Ida S, Nagaoka S, Nagata M, Matsumoto Y, Kusakabe K, Morooka S (2001) Chem Soc Jpn 11:631
28. Kotsuki H, Nishizawa H, Kitagawa S, Ochi M, Yamasaki N, Matsuoka K, Tokoroyama T (1979) Bull Chem Soc Jpn 52:544
29. Ku C-H, Wu J-J (2004) Carbon 42:2201
30. Mallika K, Komanduri R (1999) Wear 224:245
31. Welz S, Gogotsi Y, McNallan M (2003) J Appl Phys 93:4207
32. Kozai Y, Arima M (2005) Am Mineral 90:1759
33. Moore M (1985) Ind Diamond Rev 45(2):67
34. Yu Z, Flodström (1997) Diamond Relat Mater 6:81
35. Mendelssohn MJ, Milledge HJ (1995) Int Geol Rev 37(4):285
36. Fritsh E, Moore M, Rondeau B, Waggett RG (2005) J Crystal Growth 280:279
37. Kanda H, Ohsawa T, Fukunaga O, Sunagawa I (1989) J Crystal Growth 94(1):115
38. Palyanov YuN, Sokol AG, Borzdov YuM, Khokhryakov AF, Shatsky AF, Sobolev NV (1999) Diamond Relat Mater 8:1118
39. Fernandes AJS, Silva VA, Carrapichano JM, Dias GR, Silva RF, Costa FM (2001) Diamond Relat Mater 10:803
40. Malcher V, Mrška A, Kromka A, Šatka A, Janík J (2002) Curr Appl Phys 2:201
41. Teraji T, Mitani S, Wang C, Ito I (2002) J Crystal Growth 235:287
42. Sternberg M, Kaukonen M, Nieminen RM, Frauenheim Th (2001) Phys Rev B 63:165414
43. Chu CJ, Hayge RH, Margrave JL, D'evelyn MP (1992) Appl Phys Lett 61(12):1393
44. Chu CJ, D'Evelyn MP, Hayge RH, Margrave JL (1991) J Appl Phys 70(3):1695
45. Lu FX, Liu JM, Chen GC, Tang WZ, Li CM, Song JH, Tong JM (2004) Diamond Relat Mater 13:533
46. Yamasaki N (2003) J Cer Soc Jpn 111(10):709
47. Erasmus RM, Comins JD, Fish ML (2000) Diamond Relat Mater 9:600
48. Ferrari AC, Robertson J (2000) In: Proceedings of materials research society symposium, vol 593, p 299
49. Korablov S, Yamasaki N, Tohji K, Yokosawa K (2003) In: Proceedings of annual meeting of the ceramic society of Japan, Tokyo, 22–24 March 2003, p 47
50. Fang Z, Smith RL, Inomata H, Arai K (2000) J Supercrit Fluid 16:207
51. Wu J-J, Ku C-H, Wong T-C, Wu C-T, Chen K-H, Chen L-C (2005) Thin Sol Film 473(1):24
52. Yamasaki N, Korablov S, Yokosawa K (2002) In: Proceedings of conference of the Mining and Materials Processing Institute of Japan, Chiba, 28–30 March 2002, p 136
53. Redfern PC, Horner DA, Curtiss LA, Gruen DM (1996) J Phys Chem 100:11654
54. Korablov S, Yamasaki N, Tohji K, Yokosawa K, Korablov D (2006) Mater Lett 60(25–26):3041
55. Mallika K, DeVries RC, Komanduri R (1999) Thin Sol Film 339:19